Stress focusing for controlled fracture in microelectromechanical systems

Matthew A. Meitl,[a] Xue Feng, Jingyan Dong, Etienne Menard, Placid M. Ferreira, Yonggang Huang, and John A. Rogers[b]

Department of Materials Science and Engineering, Department of Mechanical Science and Engineering, Beckman Institute for Advanced Science and Technology, and Frederick Seitz Materials Research Laboratory, University of Illinois at Urbana-Champaign, Urbana, Illinois 61801

(Received 12 January 2007; accepted 20 January 2007; published online 22 February 2007)

This letter describes a strategy for controlling fracture in microelectromechanical systems (MEMSs) based on the control of corner sharpness. Studies of model MEMS structures with round (radius of approximately microns), intermediate, and sharp (<10 nm) corners demonstrate the effects of corner sharpness on the concentration of applied stress. Finite-element analysis reveals that stress distributions intensify and localize as sharpness increases, and transfer printing experiments demonstrate the influence of stress concentration on breakability. © *2007 American Institute of Physics*. [DOI: 10.1063/1.2679072]

Certain system-on-a-chip[1] and other emerging technologies in microelecromechanical systems[2–6] (MEMSs) and unconventional electronics[7–11] require the transfer of microcomponents from the substrate on which they are fabricated to another device substrate. To maintain organization, tethers and anchoring structures fix the otherwise released components in their original positions until the point of transfer, when they break away via fracture. In this letter we report the ability to control fracture via the introduction of features that focus mechanical stress at sharp corners, characterized by radii of curvature at ~10 nm scale and lower. These stress concentration points fix the centers of crack nucleation and greatly improve breakability. We examine the stress distributions around the corners with varying degrees of sharpness using finite-element analysis (FEA) and we demonstrate the utility of stress concentration in the context of transfer printing silicon microstructures using polydimethylsiloxane (PDMS) stamps.

The study begins with the fabrication of a model MEMS-like system from a silicon-on-insulator wafer (Shin-Etsu, ~2.5 μm top silicon, 1.5 μm oxide) as illustrated in Fig. 1. One of three micromachining techniques defines features in the top silicon with varying degrees of sharpness. In the first of these, photolithography and SF_6 plasma etching (Plasmatherm reactive ion etching system, 40 SCCM (SCCM denotes cubic centimeter per minute at STP) SF_6, 50 mTorr, 100 W, ~300 s) etch $\sim 170 \times 10\ \mu m^2$ beams tethered at either end to a wide, perpendicularly-oriented anchoring element via a narrow bridge. In the other two, aqueous hydroxide-based etches define similar structures. Plasma-enhanced chemical vapor deposition of 200 nm of silicon nitride followed by photolithography and dry etching (40 SCCM CHF_3, 2 SCCM O_2, 50 mTorr, 150 W,~360 s) produces a silicon nitride etch mask with geometry identical to the mask composed of photoresist for the SF_6 etching described above. The wet etchant, either 25 wt. % KOH in water or the same mixture with about 20 wt. % isopropyl alcohol added (KOH/IPA), etches the silicon within about 3 min on a hot plate set to 110 °C. After etching, exposure to concentrated hydrofluoric acid (7 min) removes the etch mask and the oxide from underneath the beams but only partially from underneath the wider anchoring elements. After rinsing with water and drying with nitrogen, the released beams sag and contact the underlying silicon at their centers. To complete the process, the beams break away from the anchoring elements via PDMS stamps (Dow-Sylgard 184).[8] A mechanical stage applies the stamp ($0.95 \times 0.95\ mm^2$) to the chip at ~54 kPa for 10 s before removal at a vertical speed of 1 cm/s. The mechanical stage provides reproducible retrieval despite the strongly rate-dependent PDMS adhesion mechanics.[8]

The three etching methods (SF_6, KOH/IPA, and KOH) produce silicon beams with different geometrical characteristics, shown in Fig. 2. SF_6 [Fig. 2(a)] undercuts the photoresist etch mask significantly, resulting in narrower beams

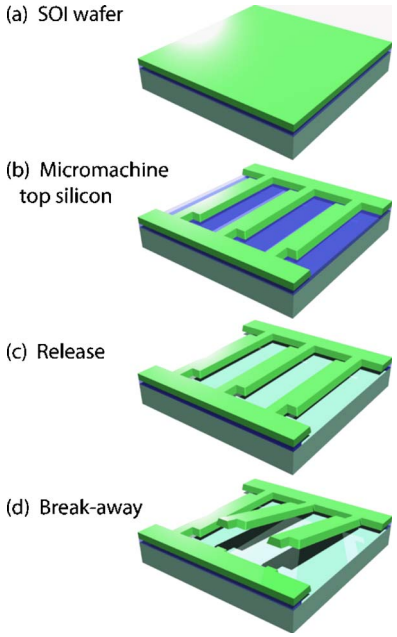

FIG. 1. (Color online) Schematic for the fabrication of "breakaway" MEMS. The process begins with a chip (a), for example, silicon on insulator (SOI). Micromachining techniques define structures in the top silicon (b), and a release process (c) renders the structures freestanding yet anchored to the original wafer. The structures then separate via fracture (d) due to an applied force.

[a]Author to whom correspondence should be addressed; present address: 1304 West Green Street, Urbana, Illinois; electronic mail: meitl@uiuc.edu
[b]Author to whom correspondence should be addressed; present address: 1304 West Green Street, Urbana, Illinois; electronic mail: jrogers@uiuc.edu

 © 2007 American Institute of Physics
Downloaded 22 Feb 2007 to 128.174.209.25. Redistribution subject to AIP license or copyright, see http://apl.aip.org/apl/copyright.jsp

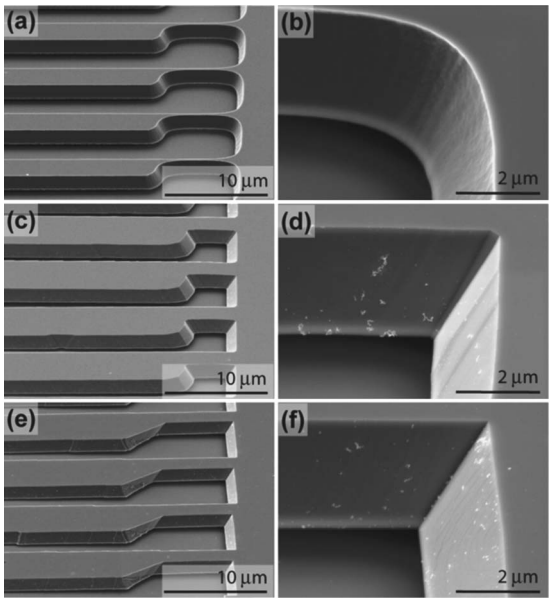

FIG. 2. SEM of structures produced by different etches. (a) Anchored beams produced by dry etching a SOI wafer in SF_6 plasma followed by release in hydrofluoric acid. (b) Magnified view revealing the critical radius of features generated by SF_6 (1.7 μm). [(c) and (d)] Beams produced by wet etching in KOH/IPA (critical radius: 0.12 μm). [(e) and (f)] Beams produced by etching in aqueous KOH (radius: 0.01 μm).

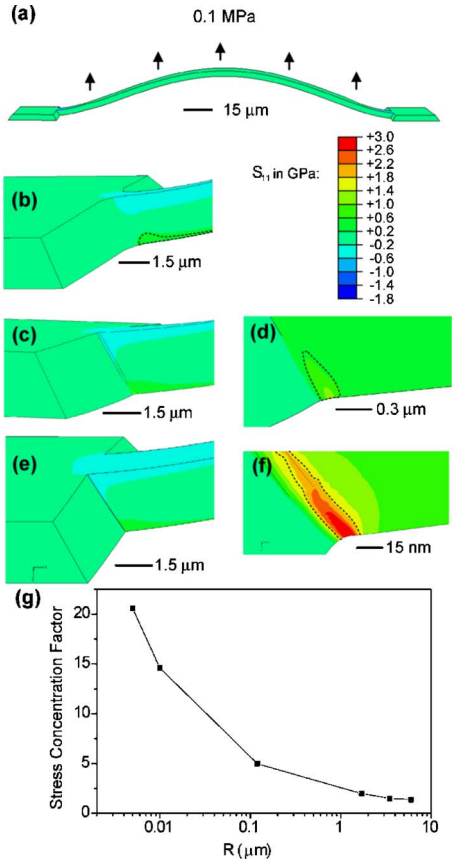

FIG. 3. (Color online) Finite-element modeling of stress concentration in breakaway MEMS structures. (a) Deflection of anchored beam structure with 0.1 MPa applied vertically. (b) Stress distribution in SF_6-etched beam (critical radius: 1.7 μm). (c) Stress distribution in beam etched in KOH/IPA (radius: 0.12 μm). (d) Magnified view of critical region in (c). (e) Stress in beam etched in aqueous KOH without IPA (radius: 0.01 μm). (f) Magnified view of critical region in (e). The dotted lines in (b), (d), and (f) outline the contours of half maximum stress. (g) Stress concentration factor as a function of critical feature radius for anchored beams with otherwise identical geometry to the KOH-etched beams.

and round corners. The roundness originates from the photolithography and the partially isotropic plasma etch. Figure 2(b) shows a magnified view of the beam-anchor joint. As viewed from normal to the chip surface, the radius of the curvature at the bottom of this joint is ~1.7 μm. In contrast, KOH/IPA produces silicon beams with greatly reduced undercutting and sharper corners [Figs. 2(c) and 2(d)]. The magnified view shows a corner that comprises two (1 1 1) planes and a third face, roughly (1 1 0), that serves as a fillet and gives the corner a radius of about 120 nm. This roundness originates from the etch mask features (radius ~1.6 μm) and decreases during etching. For example, exposure of the silicon to KOH/IPA for 4 min beyond what is required to expose the buried oxide yields a corner that, to within the resolution of our scanning electron microscope (SEM), has no fillet. The third etchant (KOH without IPA) immediately produces silicon beams with yet sharper corners [Figs. 2(e) and 2(f)]. Like KOH/IPA, the KOH etches anisotropically and exposes the (1 1 1) planes. Unlike KOH/IPA, the KOH quickly undercuts the rounded corners of the etch mask resulting in an immediate sharpening effect. The KOH produces a nonfilleted corner within 60 s, well before the buried oxide is exposed. The beam-anchor joint etched by KOH is sharper than the resolution of our SEM, giving a characteristic radius below 10 nm.

Corner sharpness plays an important role in the distribution of internal stress as the beams are lifted from the chip. To investigate the mechanics, we performed FEA using ABAQUS. In the FEA, a uniform pressure (0.1 MPa for the results presented here) pulls vertically on the detailed models closely resembling the beams and anchors etched by SF_6, KOH/IPA, and KOH. The models incorporate the intricacies of the structures described above, and the mesh is defined such that the element density is greatest near the corners to capture the stress concentration there. The smallest elements are ~1 nm and always less than 1/10 of the corner radius. The FEA is performed with the anchors fixed and the beam free to deflect. The results of the FEA are illustrated in Fig. 3. Figure 3(a) shows the deflection of a KOH-etched beam with the applied load. The deflections of the SF_6 and KOH/IPA beams are similar to those of the KOH beams. Major differences occur, however, in the distribution of the tensile stress parallel to the beam axis at the beam-anchor joints. Beam theory predicts a nominal maximum stress of 2310 times the applied pressure (0.1 MPa) for a rectangular beam with dimensions of $2.5\times10\times170$ μm^3, but the maximum stress in the SF_6 [Fig. 3(b)], KOH/IPA [Figs. 3(c) and 3(d)] and KOH [Figs. 3(e) and 3(f)] systems are 5170, 11760, and 33750 times the applied pressure, respectively. The FEA demonstrates that the corner sharpness strongly regulates the stress concentration. Figure 3(g) plots the stress concentration factor, defined as the maximum stress near the corner divided by the nominal maximum stress given by beam theory, for a series of models with varying corner radii, otherwise geometrically identical to the KOH-etched system. The stress concentration factor ranges from greater than 20 (R=5 nm) to about 1.4 at R=6 μm. In addition to producing high stress maxima, corner sharpness spatially confines the stress. For example, the sharp corners produced by KOH etching [Fig. 3(f)] induce a stress distribution with a full width at half maximum value of just 16 nm along the underside edges of the beam. The corresponding width for the

Downloaded 22 Feb 2007 to 128.174.209.25. Redistribution subject to AIP license or copyright, see http://apl.aip.org/apl/copyright.jsp

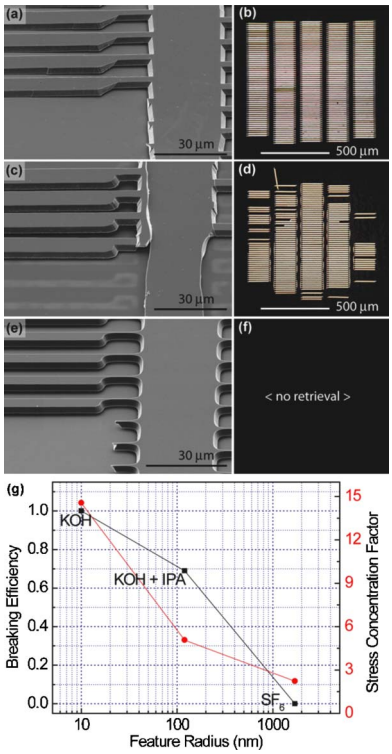

FIG. 4. (Color online) Effects of stress concentration on breakability. (a) SEM showing clean breaks of anchored silicon beams etched with KOH. (b) Assembly of the beams shown in (a) efficiently retrieved by a stamp and printed onto scotch tape. (c) Anchored silicon beams etched with KOH/IPA and retrieved using a PDMS stamp showing a poorly defined fracture zone due to reduced sharpness in the corners. (d) Reduced retrieval efficiency [relative to (b)] of the beams in (c). (e) Anchored beams produced with SF6 plasma etching with three beams removed. (f) Failed retrieval of the SF_6-etched beams. (g) plots of breaking efficiency (black squares) and stress concentration factor (red circles) vs critical feature radius for the beams produced by the three different etching methods.

KOH/IPA system is ~190 nm, and the SF_6 system has half maximum stress that extends more than 4 μm. The dotted curves in Figs. 3(b), 3(d), and 3(f) outline the half maximum stress contours of the SF_6, KOH/IPA, and KOH systems, respectively.

The stress-focusing effect governs the ability of the beams to break from the anchoring structures. Figure 4 summarizes the implications of stress focusing on breakability with images quantifying the yield of transfer printing experiments and postfracture images. Figure 4(a) shows a substrate with beams etched using KOH and removed using a PDMS stamp as described above. The very sharp corners generate stress concentrations that break the beams cleanly and easily at the beam-anchor joint, where the stress is greatest. Figure 4(b) demonstrates the effectiveness of the beam retrieval, showing a near-perfectly retrieved patch of beams printed from the PDMS onto scotch tape. No beams are missing except for a few at the edges of the patch. Figures 4(c) and 4(d) show similar images for the KOH/IPA system. Relative to KOH, the fracture location in this system is poorly defined. Fractures occur at the beam-anchor joint but frequently propagate into the anchor [Fig. 4(c)] or other parts of the beam structure, resulting in broken beams and beams that are unintentionally interconnected after retrieval [Fig. 4(d)]. FEA suggests that these defects are caused by the diffuse stress distributions in the KOH/IPA system relative to those in the KOH system. Additionally, the lower stress maxima in KOH/IPA beams make them more difficult to remove. Figure 4(d) shows that the stamping procedure retrieves only about $\frac{3}{4}$ of the beams compared to the near-perfect retrieval of the KOH beams. The effects of diffuse stress distributions are even more pronounced in the SF_6 case [Figs. 4(e) and 4(f)]. The stamping procedures that were used to break the KOH and KOH/IPA beams were entirely unsuccessful at breaking and retrieving the beams produced using SF_6 [Fig. 4(f)]. The fractures shown in Fig. 4(e) were accomplished using a more aggressive (faster and manual) PDMS stamping procedure. Figure 4(g) illustrates the strong correlation of the breakability of the three types of beams by the standardized stamping procedure to the maximum stress concentration predicted by FEA. In this figure, the breaking efficiency is defined as the number of beams retrieved by the stamping procedure relative to the number broken in the KOH system (100%, $N=299$), and the stress concentration factor is the same as defined above, each plotted versus the corner radius.

In summary, nanoscale corner sharpness in MEMS-like structures focuses applied stress and governs the ease and precision of fracture. FEA and transfer printing experiments demonstrate these effects using micromachined beams with different degrees of corner sharpness. This stress-focusing phenomenon plays a significant role in the engineering of controlled fracture sites and in the general study of fracture in materials.

This work was supported by the U.S. Department of Energy under Grant No. DEFG02-91-ER45439, the National Science Foundation under Grant No. DMI-0328162, and a graduate fellowship from the Fannie and John Hertz Foundation to one of the authors (M.A.M.).

[1] K. Banerjee, S. J. Souri, P. Kapur, and K. C. Saraswat, Proc. IEEE **89**, 602 (2001).
[2] A. Singh, D. A. Horsley, M. B. Cohn, A. P. Pisano, and R. T. Howe, J. Microelectromech. Syst. **8**, 27 (1999).
[3] N. Dechev, W. L. Cleghorn, and J. K. Mills, J. Microelectromech. Syst. **13**, 176 (2004).
[4] J. Y. Chen, L. S. Huang, C. H. Chu, and C. Peizen, J. Micromech. Microeng. **12**, 406 (2002).
[5] N. Dechev, W. L. Cleghorn, and J. K. Mills, Proc. SPIE **5344**, 134 (2004).
[6] F. F. Faheem and Y. C. Lee, Sens. Actuators, A **114**, 486 (2004).
[7] K. J. Lee, M. J. Motala, M. A. Meitl, W. R. Childs, E. Menard, A. K. Shim, J. A. Rogers, and R. G. Nuzzo, Adv. Mater. (Weinheim, Ger.) **17**, 2332 (2005).
[8] M. A. Meitl, Z. T. Zhu, V. Kumar, K. J. Lee, X. Feng, Y. Y. Huang, I. Adesida, R. G. Nuzzo, and J. A. Rogers, Nat. Mater. **5**, 33 (2006).
[9] Y. G. Sun, D. Y. Khang, F. Hua, K. Hurley, R. G. Nuzzo, and J. A. Rogers, Adv. Funct. Mater. **15**, 30 (2005).
[10] H. C. Ko, A. J. Baca, and J. A. Rogers, Nano Lett. **6**, 2318 (2006).
[11] S. Mack, M. A. Meitl, A. J. Baca, Z. T. Zhu, and J. A. Rogers, Appl. Phys. Lett. **88** 213101 (2006).

Downloaded 22 Feb 2007 to 128.174.209.25. Redistribution subject to AIP license or copyright, see http://apl.aip.org/apl/copyright.jsp